INTERNATIONAL JOURNAL FOR NUMERICAL METHODS IN FLUIDS
Int. J. Numer. Meth. Fluids 2007; **54**:1291–1312
Published online 31 January 2007 in Wiley InterScience (www.interscience.wiley.com). DOI: 10.1002/fld.1420

Orthogonality of modal bases in *hp* finite element models

V. Prabhakar and J. N. Reddy*, †

Department of Mechanical Engineering, Texas A&M University, College Station, TX 77843, U.S.A.

SUMMARY

In this paper, we exploit orthogonality of modal bases (*SIAM J. Sci. Comput.* 1999; **20**:1671–1695) used in *hp* finite element models. We calculate entries of coefficient matrix analytically without using any numerical integration, which can be computationally very expensive. We use properties of Jacobi polynomials and recast the entries of the coefficient matrix so that they can be evaluated analytically. We implement this in the context of the least-squares finite element model although this procedure can be used in other finite element formulations. In this paper, we only develop analytical expressions for rectangular elements. Spectral convergence of the L_2 least-squares functional is verified using exact solution of Kovasznay flow. Numerical results for transient flow over a backward-facing step are also presented. We also solve steady flow past a circular cylinder and show the reduction in computational cost using expressions developed herein. Copyright © 2007 John Wiley & Sons, Ltd.

Received 5 May 2005; Revised 25 October 2006; Accepted 25 October 2006

KEY WORDS: finite element method; modal bases; least-squares method; orthogonality; numerical results

1. INTRODUCTION

The past two decades have witnessed a great deal of progress in the area of computational fluid dynamics. A large number of methods have been proposed for the numerical solution of the Navier–Stokes equations governing flows of viscous incompressible fluids. Direct discretization includes finite difference and finite volume techniques, mixed finite element methods using conformal and non-conformal elements, and spectral methods. Finite element method and its derivatives (e.g. least-squares finite element model, spectral/*hp* finite element model) have gained popularity in the recent times.

*Correspondence to: J. N. Reddy, Department of Mechanical Engineering, Texas A&M University, College Station, TX 77843, U.S.A.
†E-mail: jnreddy@tamu.edu

Contract/grant sponsor: Air Force Office of Scientific Research; contract/grant number: F49620-03-1-0201

In the finite element method, we select basis functions to approximate dependent variables and perform coordinate transformation to evaluate the coefficient matrices. On the basis of polynomial order used, the finite element models can be divided into two groups: low-order expansions (order less than three) and high-order expansion (order higher than three). Most of the finite element implementations use low-order expansions because they require less computational time per degree of freedom, and convergence is achieved by refining the mesh. On the other hand, high-order expansions demonstrate exponential convergence. If high accuracy is required then we can justify using high-order expansions by the fact that the error will converge at a faster rate than the increase in the operation count. Therefore, ultimately it is more efficient to use high-order methods. Nevertheless, the cross-over point between the required accuracy and relative cost of low- and high-order methods for a given application is a point of much debate. A further argument presented for using high-order methods is the numerical diffusion and the enhanced phase properties that these schemes demonstrate [1, 2].

In the context of least-squares finite element models, low-order nodal expansions have been found to lock and reduced integration is used to obtain acceptable numerical results. In this case, resulting coefficient matrix is nearly singular. Furthermore, the numerical solution may not be smooth at the nodes and post-processing is needed to recover nodal values from the reduced integration points. Pontaza and Reddy [1, 3] presented spectral/*hp* least-squares finite element models and Prabhakar and Reddy [4] presented spectral/*hp* penalty least-squares finite element models. They combined the idea of least-squares method with spectral/*hp* methods, and the models performed well in solving Navier–Stokes equations.

Having outlined the need for high-order expansion basis, we need to decide the types of expansion bases used. Many types of high-order expansion bases can be found in the literature. Peano [5] constructed a hierarchical triangular basis using area coordinates. A variation of this construction was later developed by Szabo and Babuska [6] that introduced Legendre polynomials to avoid round-off error for high-order *p*-expansions. However, both approaches require special integration rules which are quite complicated at high polynomial order. Dubiner [7] first developed an alternative hierarchical basis for triangular domains that is based on cartesian coordinates. Dubiner's basis was implemented by Sherwin and Karniadakis [8] using a Galerkin finite element model of the Navier–Stokes equations, and it was found to be competitive in cost with the nodal basis on quadrilaterals employed in the spectral element method [9]. Warburton *et al.* [10] developed a unified description of hybrid basis functions. They developed five types of basis functions that are either modal, nodal or mixed, and which may or may not be hierarchical.

In this paper, we implement hierarchical modal bases. Hierarchical bases can lead to better conditioning of mass and coefficient matrices [11]. We implement these bases in the context of least-squares finite element model of the Navier–Stokes equations [1, 3]. As described earlier, high-order expansions require more work per degree of freedom (during Gauss quadrature). In this paper, we exploit orthogonality of Jacobi polynomials, and calculate integrals without using any numerical quadrature rule. We recast the terms of the coefficient matrix using the properties of Jacobi polynomial and evaluate them exactly. For rectangular elements, coefficient matrix entries are written in alternative forms and analytical expressions are developed to calculate them exactly. It is to be mentioned that multidimensional shape functions are constructed using tensor product of 1-D shape functions. Limitation of the procedure developed here is that it can be used for rectangular elements.

The present paper is organized as follows. In Section 2, we review the least-squares finite element formulation for the steady incompressible Navier–Stokes equations. The Navier–Stokes

DOI: 10.1002/fld

equations are recast as first-order system using vorticity as additional dependent variable, and then the finite element formulation for these first-order systems is presented. In Section 3, we present a couple of properties associated with Jacobi polynomials and use them to evaluate the entries of coefficient matrix. Then, in Sections 4 and 5 we recast entries of coefficient matrix for 1-D and multidimensional cases and evaluate them analytically. We implement primary boundary conditions by inverting mass matrix, description of which is given in Section 6. In Section 7, we present space–time decoupled least-squares formulation. Numerical results are presented in Section 8. The spectral convergence is verified using the Kovasznay flow solution. Numerical results are presented for transient 2-D flow over a backward-facing step. We compare results with the benchmark solution of Gartling [12] and Pontaza and Reddy [3]. Lastly, we consider the flow past a circular cylinder at low Reynolds number and compare the predicted surface pressure distribution with the experimental measurements of Grove *et al.* [13].

2. LEAST-SQUARES FINITE ELEMENT FORMULATION

The steady incompressible Navier–Stokes equations in dimensionless form can be written as follows:

$$(\mathbf{u}\cdot\nabla)\mathbf{u}+\nabla p-\frac{1}{Re}\nabla\cdot[(\nabla\mathbf{u})+(\nabla\mathbf{u})^{\mathrm{T}}]=\mathbf{f}\quad\text{in }\Omega \tag{1}$$

$$\nabla\cdot\mathbf{u}=0\quad\text{in }\Omega \tag{2}$$

$$\mathbf{u}=\mathbf{u}^{s}\quad\text{on }\Gamma_u \tag{3}$$

$$\hat{\mathbf{n}}\cdot\underline{\boldsymbol{\sigma}}=\mathbf{f}^{s}\quad\text{on }\Gamma_f \tag{4}$$

where $\mathbf{u}(\mathbf{x})$ is the velocity vector, $p(\mathbf{x})$ is the pressure, $\underline{\boldsymbol{\sigma}}=-p\underline{\mathbf{I}}+1/Re[(\nabla\mathbf{u})+(\nabla\mathbf{u})^{\mathrm{T}}]$ is the total stress, $\mathbf{f}$ is a dimensionless force, $\hat{\mathbf{n}}$ is the outward unit normal on the boundary of Ω, $\mathbf{u}^{s}$ is the prescribed velocity on the boundary Γ_u, and $\mathbf{f}^{s}$ is the prescribed boundary stress on the boundary Γ_f, $\Gamma=\Gamma_u\cup\Gamma_f$ and $\Gamma_u\cap\Gamma_f=\emptyset$, and Re is the Reynolds number.

To reduce the system to first order, we introduce vorticity vector as an independent variable. We make use of the vector identity

$$\nabla\times\nabla\times\mathbf{u}=-\nabla^2\mathbf{u}+\nabla(\nabla\cdot\mathbf{u})$$

Then determining the solution of the stationary Navier–Stokes equations, Equations (1)–(4), can now be stated as:

find the velocity $\mathbf{u}(\mathbf{x})$, pressure $p(\mathbf{x})$, and vorticity $\boldsymbol{\omega}(\mathbf{x})$ such that

$$(\mathbf{u}\cdot\nabla)\mathbf{u}+\nabla p+\frac{1}{Re}\nabla\times\boldsymbol{\omega}=\mathbf{f}\quad\text{in }\Omega \tag{5}$$

$$\boldsymbol{\omega}-\nabla\times\mathbf{u}=\mathbf{0}\quad\text{in }\Omega \tag{6}$$

$$\nabla\cdot\mathbf{u}=0\quad\text{in }\Omega \tag{7}$$

$$\mathbf{u}=\mathbf{u}^{s}\quad\text{on }\Gamma_u \tag{8}$$

$$\boldsymbol{\omega}=\boldsymbol{\omega}^{s}\quad\text{on }\Gamma_\omega \tag{9}$$

DOI: 10.1002/fld

The L_2 least-squares functional associated with the velocity–pressure–vorticity equations presented above is given by

$$\mathscr{J}(\mathbf{u}, p, \boldsymbol{\omega}; \mathbf{f}) = \frac{1}{2}\left(\left\|(\mathbf{u}\cdot\nabla)\mathbf{u} + \nabla p + \frac{1}{Re}\nabla\times\boldsymbol{\omega} - \mathbf{f}\right\|_0^2 + \|\boldsymbol{\omega} - \nabla\times\mathbf{u}\|_0^2 + \|\nabla\cdot\mathbf{u}\|_0^2\right) \tag{10}$$

The least-squares principle can be stated as one of finding $(\mathbf{u}, p, \boldsymbol{\omega})\in\mathbf{X}$ such that for all $(\mathbf{v}, q, \boldsymbol{\psi})\in\mathbf{X}$

$$\mathscr{J}(\mathbf{u}, p, \boldsymbol{\omega}; \mathbf{f}) \leqslant \mathscr{J}(\mathbf{v}, q, \boldsymbol{\psi}; \mathbf{f}) \tag{11}$$

holds, where

$$\mathbf{X} = \{(\mathbf{u}, p, \boldsymbol{\omega}) \in \mathbf{H}_0^1(\Omega)\times H^1(\Omega)\cap \bar{L}_2(\Omega)\times\mathbf{H}^1(\Omega)\}$$

The Euler–Lagrange equations associated with this minimum principle are equivalent to the following variational problem: find $(\mathbf{u}, p, \boldsymbol{\omega}) \in \mathbf{X}$ such that for all $(\mathbf{v}, q, \boldsymbol{\psi}) \in \mathbf{X}$

$$\mathscr{B}((\mathbf{u}, p, \boldsymbol{\omega}), (\mathbf{v}, q, \boldsymbol{\psi})) = \mathscr{F}((\mathbf{v}, q, \boldsymbol{\psi})) \tag{12}$$

where

$$\begin{aligned}
&\mathscr{B}((\mathbf{u}, p, \boldsymbol{\omega}), (\mathbf{v}, q, \boldsymbol{\psi}))\\
&\quad= \int_\Omega \left((\mathbf{u_0}\cdot\nabla)\mathbf{u} + \nabla p + \frac{1}{Re}\nabla\times\boldsymbol{\omega}\right)\cdot\left((\mathbf{u_0}\cdot\nabla)\mathbf{v} + \nabla q + \frac{1}{Re}\nabla\times\boldsymbol{\psi}\right)\mathrm{d}\Omega\\
&\qquad+ \int_\Omega (\boldsymbol{\omega} - \nabla\times\mathbf{u})\cdot(\boldsymbol{\psi} - \nabla\times\mathbf{v})\,\mathrm{d}\Omega + \int_\Omega (\nabla\cdot\mathbf{u})(\nabla\cdot\mathbf{v})\,\mathrm{d}\Omega
\end{aligned}$$

and

$$\mathscr{F}((\mathbf{v}, q, \boldsymbol{\psi})) = \int_\Omega \mathbf{f}\cdot\left((\mathbf{u_0}\cdot\nabla)\mathbf{v} + \nabla q + \frac{1}{Re}\nabla\times\boldsymbol{\psi}\right)\mathrm{d}\Omega$$

We have used Picard method, where we linearize equations first and then minimize the least-squares functional.

2.1. Finite element model

The finite element model is obtained by restricting (12) to a finite-dimensional subspace $\mathbf{X}_{hp}$ of the space $\mathbf{X}$. Then, the discrete least-squares finite element model for the incompressible Navier–Stokes equations is given by the following discrete variational problem:

find $(\mathbf{u}^{hp}, p^{hp}, \boldsymbol{\omega}^{hp}) \in \mathbf{X}_{hp}$ such that for all $(\mathbf{v}^{hp}, q^{hp}, \boldsymbol{\psi}^{hp}) \in \mathbf{X}_{hp}$

$$\mathscr{B}((\mathbf{u}^{hp}, p^{hp}, \boldsymbol{\omega}^{hp}), (\mathbf{v}^{hp}, q^{hp}, \boldsymbol{\psi}^{hp})) = \mathscr{F}((\mathbf{v}^{hp}, q^{hp}, \boldsymbol{\psi}^{hp})) \tag{13}$$

DOI: 10.1002/fld

For details, see Pontaza and Reddy [3]. This procedure leads to the following system of equations:

$$\begin{pmatrix} [S^{11}+S^{22}] & [S^{12}-S^{21}] & [0] & [S^{20}] \\ [S^{21}-S^{12}] & [S^{11}+S^{22}] & [0] & -[S^{10}] \\ [0] & [0] & [S^{11}+S^{22}] & \dfrac{1}{Re}[S^{12}-S^{21}] \\ [S^{02}] & -[S^{01}] & \dfrac{1}{Re}[S^{21}-S^{12}] & \dfrac{1}{Re^2}[S^{11}+S^{22}]+[S^{00}] \end{pmatrix} \begin{pmatrix} \{v_x\} \\ \{v_y\} \\ \{P\} \\ \{\omega_z\} \end{pmatrix}$$

$$+ \begin{pmatrix} [C^{00}(\mathbf{v})] & [0] & [C^{01}(\mathbf{v})] & \dfrac{1}{Re}[C^{02}(\mathbf{v})] \\ [0] & [C^{00}(\mathbf{v})] & [C^{02}(\mathbf{v})] & -\dfrac{1}{Re}[C^{01}(\mathbf{v})] \\ [C^{10}(\mathbf{v})] & [C^{20}(\mathbf{v})] & [0] & [0] \\ \dfrac{1}{Re}[C^{20}(\mathbf{v})] & -\dfrac{1}{Re}[C^{10}(\mathbf{v})] & [0] & [0] \end{pmatrix} \begin{pmatrix} \{v_x\} \\ \{v_y\} \\ \{P\} \\ \{\omega_z\} \end{pmatrix} = \begin{pmatrix} \{F^1\} \\ \{F^2\} \\ \{F^3\} \\ \{F^4\} \end{pmatrix}$$

$$C_{ij}^{00}(\mathbf{v}) = \int_{\Omega^e} \mathscr{C}_i \mathscr{C}_j \, \mathrm{d}x \, \mathrm{d}y, \quad \mathscr{C}_i = v_x \frac{\partial \psi_i}{\partial x} + v_y \frac{\partial \psi_i}{\partial y}$$

$$C_{ij}^{01}(\mathbf{v}) = \int_{\Omega^e} \mathscr{C}_i \frac{\partial \psi_j}{\partial x} \, \mathrm{d}x \, \mathrm{d}y, \quad C_{ij}^{02}(\mathbf{v}) = \int_{\Omega^e} \mathscr{C}_i \frac{\partial \psi_j}{\partial y} \, \mathrm{d}x \, \mathrm{d}y$$

$$C_{ij}^{10}(\mathbf{v}) = \int_{\Omega^e} \frac{\partial \psi_i}{\partial x} \mathscr{C}_j \, \mathrm{d}x \, \mathrm{d}y, \quad C_{ij}^{20}(\mathbf{v}) = \int_{\Omega^e} \frac{\partial \psi_i}{\partial y} \mathscr{C}_j \, \mathrm{d}x \, \mathrm{d}y$$

$$S_{ij}^{00} = \int_{\Omega^e} \psi_i \psi_j \, \mathrm{d}\Omega$$

$$S_{ij}^{01} = \int_{\Omega^e} \psi_i \frac{\partial \psi_j}{\partial x} \, \mathrm{d}x \, \mathrm{d}y, \quad S_{ij}^{02} = \int_{\Omega^e} \psi_i \frac{\partial \psi_j}{\partial y} \, \mathrm{d}x \, \mathrm{d}y$$

$$S_{ij}^{10} = \int_{\Omega^e} \frac{\partial \psi_i}{\partial x} \psi_j \, \mathrm{d}x \, \mathrm{d}y, \quad S_{ij}^{20} = \int_{\Omega^e} \frac{\partial \psi_i}{\partial y} \psi_j \, \mathrm{d}x \, \mathrm{d}y$$

$$S_{ij}^{11} = \int_{\Omega^e} \frac{\partial \psi_i}{\partial x} \frac{\partial \psi_j}{\partial x} \, \mathrm{d}x \, \mathrm{d}y, \quad S_{ij}^{22} = \int_{\Omega^e} \frac{\partial \psi_i}{\partial y} \frac{\partial \psi_j}{\partial y} \, \mathrm{d}x \, \mathrm{d}y$$

$$S_{ij}^{12} = \int_{\Omega^e} \frac{\partial \psi_i}{\partial x} \frac{\partial \psi_j}{\partial y} \, \mathrm{d}x \, \mathrm{d}y, \quad S_{ij}^{21} = \int_{\Omega^e} \frac{\partial \psi_i}{\partial y} \frac{\partial \psi_j}{\partial x} \, \mathrm{d}x \, \mathrm{d}y$$

DOI: 10.1002/fld

$$F_i^1 = \int_{\Omega^e} \mathscr{C}_i f_x \, \mathrm{d}x \, \mathrm{d}y$$

$$F_i^2 = \int_{\Omega^e} \mathscr{C}_i f_y \, \mathrm{d}x \, \mathrm{d}y$$

$$F_i^3 = \int_{\Omega^e} \left(\frac{\partial \psi_i}{\partial x} f_x + \frac{\partial \psi_i}{\partial y} f_y \right) \mathrm{d}x \, \mathrm{d}y$$

$$F_i^4 = \int_{\Omega^e} \frac{1}{Re} \left(\frac{\partial \psi_i}{\partial y} f_x - \frac{\partial \psi_i}{\partial x} f_y \right) \mathrm{d}x \, \mathrm{d}y$$

We proceed to develop a discrete problem by choosing appropriate finite element subspaces for the velocity, pressure and vorticity. There are no restrictive compatibility conditions on the discrete spaces, so we choose the same finite element subspace for each of the primary variables. The only requirement on the approximating spaces is that we choose continuous piecewise polynomials.

Modal expansion: In the standard interval $\Omega_{\mathrm{st}} = \{\xi | -1 < \xi < 1\}$ modal expansions are defined as

$$\psi_i(\xi) = \begin{cases} \dfrac{1-\xi}{2}, & i = 1 \\ \left(\dfrac{1-\xi}{2}\right)\left(\dfrac{1+\xi}{2}\right) P_{p-2}^{\alpha,\beta}, & 2 \leqslant i \leqslant p, \quad p \geqslant 2 \\ \dfrac{1+\xi}{2}, & i = p+1 \end{cases} \tag{14}$$

In definition (14), $P_p^{\alpha,\beta}$ are the Jacobi polynomials of order p. We use ultraspheric polynomials corresponding to the choice $\alpha = \beta = 1$. Multidimensional modal expansions are constructed by taking tensor product of 1-D modal expansions. An important property of Jacobi polynomials is their orthogonal relationship given by the following equation:

$$\int_{-1}^{1} (1-x)^{\alpha} (1+x)^{\beta} P_p^{\alpha,\beta}(x) P_q^{\alpha,\beta}(x) \, \mathrm{d}x = C \delta_{pq} \tag{15}$$

where the value of C depends on α, β and p, and it has the value

$$C = \frac{2^{\alpha+\beta+1}}{2p+\alpha+\beta+1} \frac{\Gamma(p+\alpha+1)\Gamma(p+\beta+1)}{p!\Gamma(p+\alpha+\beta+1)} \tag{16}$$

Other notable property is that the multidimensional shape functions are constructed by taking tensor product of 1-D shape functions. These two properties make the computation of coefficient matrix very fast. The shape functions in 2-D are given below.

Interior modes:

$$\phi_{mn}^{\mathrm{interior}} = \left(\frac{1+\xi}{2}\right)\left(\frac{1-\xi}{2}\right) P_{m-1}^{1,1}(\xi) \left(\frac{1+\eta}{2}\right)\left(\frac{1-\eta}{2}\right) P_{n-1}^{1,1}(\eta)$$

Vertex modes:

$$\phi^{\mathrm{vertex}_1} = \left(\frac{1-\xi}{2}\right)\left(\frac{1-\eta}{2}\right)$$

DOI: 10.1002/fld

$$\phi^{\text{vertex}_2} = \left(\frac{1+\xi}{2}\right)\left(\frac{1-\eta}{2}\right)$$
$$\phi^{\text{vertex}_3} = \left(\frac{1+\xi}{2}\right)\left(\frac{1+\eta}{2}\right)$$
$$\phi^{\text{vertex}_4} = \left(\frac{1-\xi}{2}\right)\left(\frac{1+\eta}{2}\right)$$

Edge modes:

$$\phi_m^{\text{edge}_1} = \left(\frac{1+\xi}{2}\right)\left(\frac{1-\xi}{2}\right) P_{m-1}^{1,1}(\xi)\left(\frac{1-\eta}{2}\right)$$
$$\phi_n^{\text{edge}_2} = \left(\frac{1+\xi}{2}\right)\left(\frac{1-\eta}{2}\right)\left(\frac{1+\eta}{2}\right) P_{n-1}^{1,1}(\eta)$$
$$\phi_m^{\text{edge}_3} = \left(\frac{1+\xi}{2}\right)\left(\frac{1-\xi}{2}\right) P_{m-1}^{1,1}(\xi)\left(\frac{1+\eta}{2}\right)$$
$$\phi_n^{\text{edge}_4} = \left(\frac{1-\xi}{2}\right)\left(\frac{1-\eta}{2}\right)\left(\frac{1+\eta}{2}\right) P_{n-1}^{1,1}(\eta)$$

Figure 1 shows 1-D modal expansions of order 5. Expansion modes ψ_0 and ψ_P are the same as the linear finite element expansion. These are boundary modes since they are the only modes

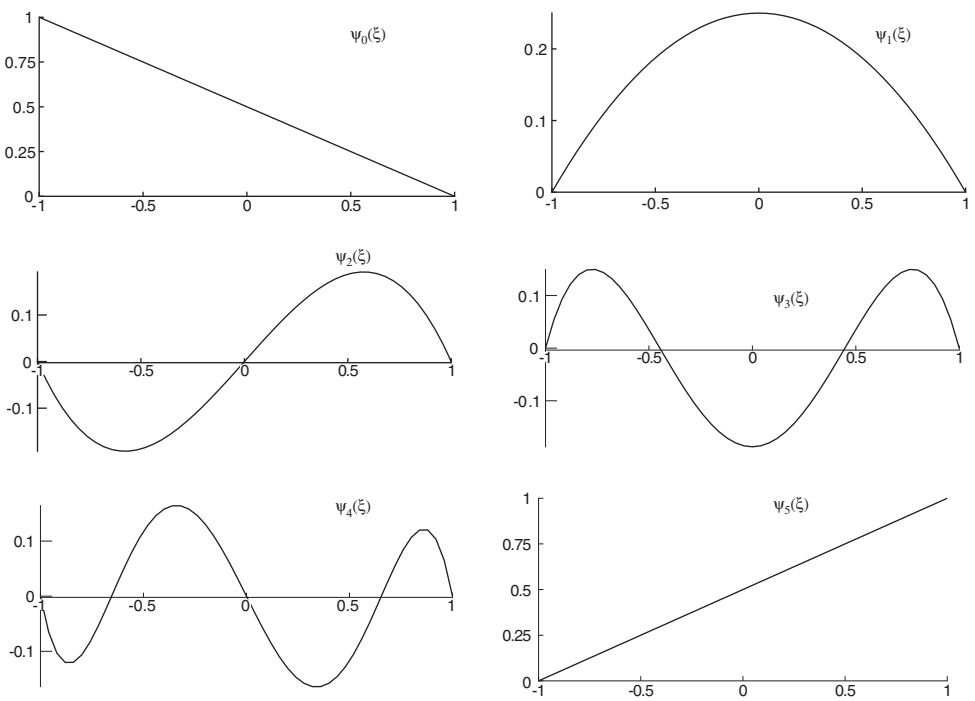

Figure 1. Shape of modal expansion modes for a polynomial order of $P = 5$.

DOI: 10.1002/fld

which have magnitude at the ends of the interval. The remaining interior modes are zero at the ends of the interval and increase in polynomial order as is typical in a hierarchical expansion. This setting helps implementing boundary conditions.

3. ORTHOGONALITY OF MODAL BASES

Modal bases defined above consist of Jacobi polynomials which are orthogonal polynomials satisfying condition (15). In Figure 2, non-zero entries of (ψ_i, ψ_j), $(\psi_i, \mathrm{d}\psi_j/\mathrm{d}\xi)$ and $(\mathrm{d}\psi_i/\mathrm{d}\xi, \mathrm{d}\psi_j/\mathrm{d}\xi)$ in 1-D for $P = 9$ are plotted, where

$$(\psi_i, \psi_j) = \int \psi_i \psi_j \, \mathrm{d}\xi \tag{17}$$

etc.; (ψ_i, ψ_j) has 32 non-zero entries out of 100. Rest of the entries are zero by the virtue of orthogonality of Jacobi polynomials; $(\psi_i, \mathrm{d}\psi_j/\mathrm{d}\xi)$ has 22 non-zero entries while $(\mathrm{d}\psi_i/\mathrm{d}\xi, \mathrm{d}\psi_j/\mathrm{d}\xi)$ has 12 non-zero entries. Analytical expressions will be developed to compute these non-zero entries without using any quadrature rule.

In Figure 3, non-zero entries of (ψ_i, ψ_j), $(\psi_i, \partial\psi_j/\partial\xi)$, $(\partial\psi_i/\partial\xi, \partial\psi_j/\partial\eta)$, $(\partial\psi_i/\partial\xi, \partial\psi_j/\partial\xi)$ in 2-D for $P = 9$ are plotted. In 2-D, (ψ_i, ψ_j), $(\psi_i, \partial\psi_j/\partial\xi)$, $(\partial\psi_i/\partial\xi, \partial\psi_j/\partial\eta)$, $(\partial\psi_i/\partial\xi, \partial\psi_j/\partial\xi)$

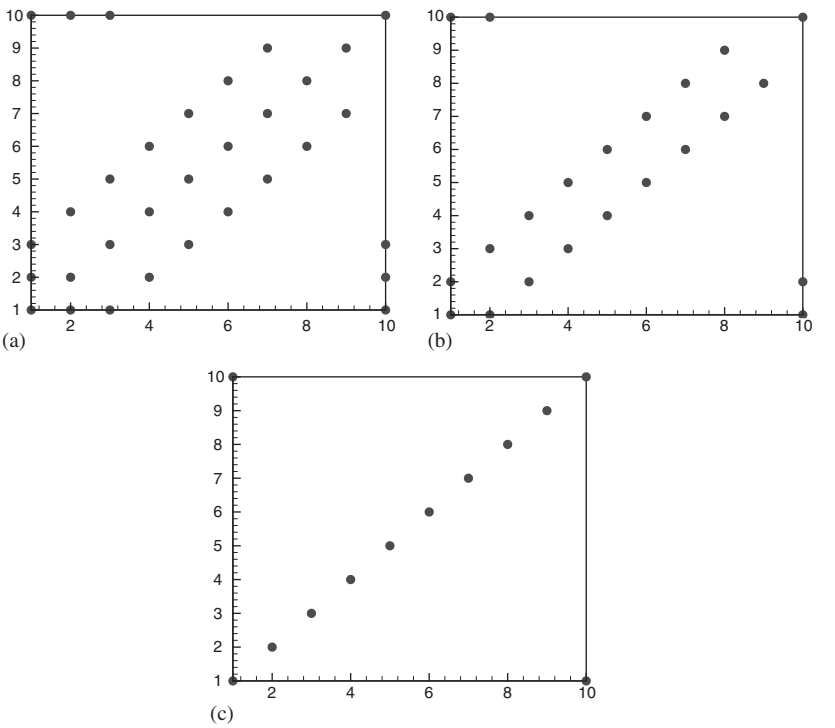

Figure 2. Non-zero entries of: (a) (ψ_i, ψ_j); (b) $(\psi_i, \mathrm{d}\psi_j/\mathrm{d}\xi)$; and (c) $(\mathrm{d}\psi_i/\mathrm{d}\xi, \mathrm{d}\psi_j/\mathrm{d}\xi)$.

DOI: 10.1002/fld

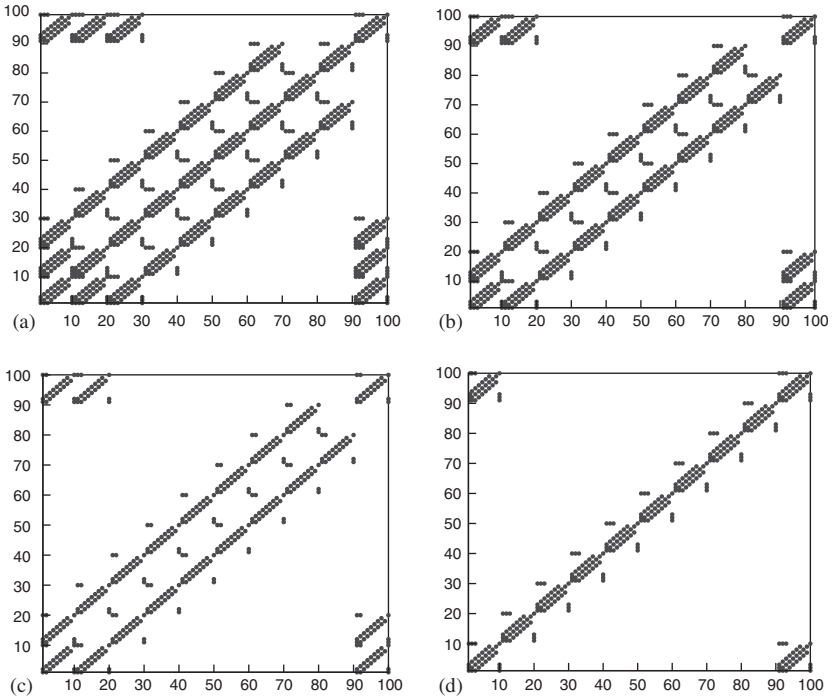

Figure 3. Non-zero entries of: (a) (ψ_i, ψ_j); (b) $(\psi_i, \mathrm{d}\psi_j/\mathrm{d}\xi)$; (c) $(\mathrm{d}\psi_i/\mathrm{d}\xi, \mathrm{d}\psi_j/\mathrm{d}\eta)$; and (d) $(\mathrm{d}\psi_i/\mathrm{d}\xi, \mathrm{d}\psi_j/\mathrm{d}\xi)$.

have 1024, 704, 484 and 384 non-zero entries, respectively, out of 10 000. These entries can be computed analytically for rectangular elements.

To exploit these orthogonality relationships while computing coefficient matrix, we need to recast stiffness matrix entries in a slightly different form. We will first state the following relationships which will be useful later. For a proof of these equalities, see [14].

Relation 1
All Jacobi polynomials, $P_n^{\alpha,\beta}(x)$, satisfy a three-term recurrence relation of the form

$$x P_n^{\alpha,\beta}(x) = a_{n-1,n}^{\alpha,\beta} P_{n-1}^{\alpha,\beta}(x) + a_{n,n}^{\alpha,\beta} P_n^{\alpha,\beta}(x) + a_{n+1,n}^{\alpha,\beta} P_{n+1}^{\alpha,\beta}(x) \tag{18}$$

where $a^{\alpha,\beta}$ depends only on α, β and n. For $\alpha = \beta = 1$, $a_{n,n}^{\alpha,\beta} = 0$ and the above equation can be written as

$$x P_n^{\alpha,\beta}(x) = a_{n-1,n}^{\alpha,\beta} P_{n-1}^{\alpha,\beta}(x) + a_{n+1,n}^{\alpha,\beta} P_{n+1}^{\alpha,\beta}(x) \tag{19}$$

or, for the sake of compactness, we rewrite the above equation by dropping α and β as we consider $\alpha = \beta = 1$ only

$$x P_n(x) = a_1(n) P_{n-1}(x) + a_2(n) P_{n+1}(x) \tag{20}$$

DOI: 10.1002/fld

where

$$a_1(n) = \frac{n+1}{2n+3} \tag{21}$$

and

$$a_2(n) = \frac{(n+1)(n+3)}{(n+2)(2n+3)} \tag{22}$$

Relation 2
All Jacobi polynomials, $P_n^{\alpha,\beta}(x)$, satisfy a three-term recurrence relation of the form

$$(1-x^2)\frac{\mathrm{d}P_n^{\alpha,\beta}(x)}{\mathrm{d}x} = c_{n-1,n}^{\alpha,\beta} P_{n-1}^{\alpha,\beta}(x) + c_{n,n}^{\alpha,\beta} P_n^{\alpha,\beta}(x) + c_{n+1,n}^{\alpha,\beta} P_{n+1}^{\alpha,\beta}(x) \tag{23}$$

where $c^{\alpha,\beta}$ depends only on α, β and n. For $\alpha=\beta=1$, $c_{n,n}^{\alpha,\beta}=0$ and the above equation can be written as

$$(1-x^2)\frac{\mathrm{d}P_n^{\alpha,\beta}(x)}{\mathrm{d}x} = c_{n-1,n}^{\alpha,\beta} P_{n-1}^{\alpha,\beta}(x) + c_{n+1,n}^{\alpha,\beta} P_{n+1}^{\alpha,\beta}(x) \tag{24}$$

Again, for the sake of compactness, we rewrite the above equation by dropping α and β and considering $\alpha=\beta=1$ only

$$(1-x^2)\frac{\mathrm{d}P_n(x)}{\mathrm{d}x} = c_1(n) P_{n-1}(x) + c_2(n) P_{n+1}(x) \tag{25}$$

where

$$c_1(n) = \frac{(n+1)(n+3)}{(2n+3)} \tag{26}$$

and

$$c_2(n) = \frac{2n(n+1)(n+3)}{(2n+3)(2n+4)} \tag{27}$$

4. ONE-DIMENSIONAL CASE

Let us recast entries of coefficient matrix using the following relationships:

$$\int \psi_p \psi_q \,\mathrm{d}\xi = \int \frac{(1-\xi)}{2}\frac{(1+\xi)}{2} P_p \frac{(1-\xi)}{2}\frac{(1+\xi)}{2} P_q \,\mathrm{d}\xi$$

$$= \frac{1}{16}\int (1-\xi)(1+\xi) P_p P_q \,\mathrm{d}\xi - \int (1-\xi)(1+\xi)\xi^2 P_p P_q \,\mathrm{d}\xi$$

DOI: 10.1002/fld

$$
\begin{aligned}
\xi^2 P_q &= \xi[\xi P_q] \\
&= [a_1(q)\xi P_{q-1} + a_2(q)\xi P_{q+1}] \\
&= a_1(q)[a_1(q-1)P_{q-2} + a_2(q-1)P_q] + a_2(q)[a_1(q+1)P_q + a_2(q+1)P_{q+2}] \\
&= a_1(q)a_1(q-1)P_{q-2} + [a_1(q)a_2(q-1) + a_2(q)a_1(q+1)]P_q \\
&\quad + a_2(q)a_2(q+1)P_{q+2}
\end{aligned}
$$

$$
\begin{aligned}
\int (1-\xi)(1+\xi)\xi^2 P_p P_q \,\mathrm{d}\xi &= a_1(q)a_1(q-1)\delta_{p,q-2}C_1 \\
&\quad + [a_1(q)a_2(q-1) + a_2(q)a_1(q+1)]\delta_{p,q}C_2 \\
&\quad + a_2(q)a_2(q+1)\delta_{p,q+2}C_3
\end{aligned}
$$

$$
\begin{aligned}
\int \psi_p \frac{\mathrm{d}\psi_q}{\mathrm{d}\xi}\,\mathrm{d}\xi &= \frac{1}{16}\int (1-\xi)(1+\xi)P_p \frac{\mathrm{d}[(1-\xi^2)P_q]}{\mathrm{d}\xi} \\
&= \frac{1}{16}\int (1-\xi)(1+\xi)P_p\left[(1-\xi^2)\frac{\mathrm{d}P_q}{\mathrm{d}\xi} - P_q 2\xi\right]\mathrm{d}\xi \\
&= \frac{1}{16}\int (1-\xi)(1+\xi)P_p(1-\xi^2)\frac{\mathrm{d}P_q}{\mathrm{d}\xi}\,\mathrm{d}\xi \\
&\quad - \frac{2}{16}\int (1-\xi)(1+\xi)P_p\xi P_q \,\mathrm{d}\xi
\end{aligned}
$$

$$
\begin{aligned}
A &= \int (1-\xi)(1+\xi)P_p[c_1(q)P_{q-1} + c_2(q)P_{q+1}]\,\mathrm{d}\xi \\
&= c_1(q)\delta_{p,q-1}C_1 + c_2(q)\delta_{p,q+1}C_2 \\
B &= \int (1-\xi)(1+\xi)P_p[a_1(q)P_{q-1} + a_2(q)P_{q+1}]\,\mathrm{d}\xi \\
&= a_1(q)\delta_{p,q-1}C_1 + a_2(q)\delta_{p,q+1}C_2
\end{aligned}
$$

$$
\int \psi_p \frac{\mathrm{d}\psi_q}{\mathrm{d}\xi}\,\mathrm{d}\xi = \frac{A-2B}{16}
$$

Here, C_1, C_2 and C_3 are given by Equation (16). We calculate $(\mathrm{d}\psi/\mathrm{d}\xi, \mathrm{d}\psi/\mathrm{d}\xi)$ term using the Gauss quadrature.

DOI: 10.1002/fld

5. MULTIDIMENSIONAL CASE

One of the notable property of modal bases used here is that multidimensional basis functions are constructed by taking tensor product of 1-D basis functions. So they can be separated. Separation is particularly easy when we use orthogonal grid. For rectangular elements jacobian matrix is of the form (see, Reddy [15, 16])

$$J = \begin{pmatrix} \dfrac{h_1}{2} & 0 \\ 0 & \dfrac{h_2}{2} \end{pmatrix}$$

and global derivatives of shape functions are

$$\begin{pmatrix} \dfrac{\partial \psi_i^{\mathrm{e}}}{\partial x} \\ \dfrac{\partial \psi_i^{\mathrm{e}}}{\partial y} \end{pmatrix} = J^{-1} \begin{pmatrix} \dfrac{\partial \psi_i^{\mathrm{e}}}{\partial \xi} \\ \dfrac{\partial \psi_i^{\mathrm{e}}}{\partial \eta} \end{pmatrix} = \begin{pmatrix} \dfrac{2}{h_1} \dfrac{\partial \psi_i^{\mathrm{e}}}{\partial \xi} \\ \dfrac{2}{h_2} \dfrac{\partial \psi_i^{\mathrm{e}}}{\partial \eta} \end{pmatrix}$$

where $\partial \psi_i^{\mathrm{e}}/\partial \xi$ and $\partial \psi_i^{\mathrm{e}}/\partial \eta$ are local derivatives of shape functions. We will use this representation to develop analytical expressions of entries of coefficient matrix.

Multidimensional shape functions are constructed by taking the tensor product of 1-D shape function

$$\phi_i(\xi, \eta) \to \phi_{p,q}(\xi, \eta) = \psi_p(\xi)\psi_q(\eta)$$
$$\phi_j(\xi, \eta) \to \phi_{r,s}(\xi, \eta) = \psi_r(\xi)\psi_s(\eta)$$
$$\phi_k(\xi, \eta) \to \phi_{m,n}(\xi, \eta) = \psi_m(\xi)\psi_n(\eta)$$

The entries of the coefficient matrix can now be rewritten as

$$\int \phi_i \phi_j \, \mathrm{d}x \, \mathrm{d}y = \int \phi_i(\xi, \eta)\phi_j(\xi, \eta) J \, \mathrm{d}\xi \, \mathrm{d}\eta$$
$$= J \int \psi_p(\xi)\psi_r(\xi) \, \mathrm{d}\xi \int \psi_q(\eta)\psi_s(\eta) \, \mathrm{d}\eta$$

$$\int \phi_i \frac{\partial \phi_j}{\partial x} \, \mathrm{d}x \, \mathrm{d}y = \int \phi_i(\xi, \eta) \frac{2}{h_1} \frac{\partial \phi_j(\xi, \eta)}{\partial \xi} J \, \mathrm{d}\xi \, \mathrm{d}\eta$$
$$= J \frac{2}{h_1} \int \psi_p(\xi) \frac{\partial \psi_r(\xi)}{\partial \xi} \, \mathrm{d}\xi \int \psi_q(\eta)\psi_s(\eta) \, \mathrm{d}\eta$$

$$\int \frac{\partial \phi_i}{\partial x} \frac{\partial \phi_j}{\partial x} \, \mathrm{d}x \, \mathrm{d}y = \int \frac{2}{h_1} \frac{\partial \phi_i(\xi, \eta)}{\partial \xi} \frac{2}{h_1} \frac{\partial \phi_j(\xi, \eta)}{\partial \xi} J \, \mathrm{d}\xi \, \mathrm{d}\eta$$
$$= J \frac{4}{h_1^2} \int \frac{\partial \psi_p(\xi)}{\partial \xi} \frac{\partial \psi_r(\xi)}{\partial \xi} \, \mathrm{d}\xi \int \psi_q(\eta)\psi_s(\eta) \, \mathrm{d}\eta$$

DOI: 10.1002/fld

$$\int \frac{\partial \phi_i}{\partial x}\frac{\partial \phi_j}{\partial y}\,\mathrm{d}x\,\mathrm{d}y = \int \frac{2}{h_1}\frac{\partial \phi_i(\xi,\eta)}{\partial \xi}\frac{2}{h_2}\frac{\partial \phi_j(\xi,\eta)}{\partial \eta}J\,\mathrm{d}\xi\,\mathrm{d}\eta$$

$$= J\frac{4}{h_1 h_2}\int \frac{\partial \psi_p(\xi)}{\partial \xi}\psi_r(\xi)\,\mathrm{d}\xi \int \psi_q(\eta)\frac{\partial \psi_s(\eta)}{\partial \eta}\,\mathrm{d}\eta$$

All these 1-D integrals can be calculated analytically using expressions developed in the previous section.

Nonlinear term $C_{ij}^{02}(\mathbf{v})$ can be written as

$$\int \mathscr{C}_i \frac{\partial \phi_j}{\partial y}\,\mathrm{d}x\,\mathrm{d}y = \int \left(U\frac{\partial \phi_i}{\partial x} + V\frac{\partial \phi_i}{\partial y}\right)\frac{\partial \phi_j}{\partial y}\,\mathrm{d}x\,\mathrm{d}y$$

$$= \int \left(U\frac{\partial \phi_i}{\partial \xi}\frac{2}{h_1} + V\frac{\partial \phi_i}{\partial \eta}\frac{2}{h_2}\right)\frac{\partial \phi_j}{\partial \eta}\frac{2}{h_2}J\,\mathrm{d}\xi\,\mathrm{d}\eta$$

$$= \int \sum U_k\phi_k\frac{\partial \phi_i}{\partial \xi}\frac{2}{h_1}\frac{2}{h_2}\frac{\partial \phi_j}{\partial \eta}J\,\mathrm{d}\xi\,\mathrm{d}\eta + \int \sum V_k\phi_k\frac{\partial \phi_i}{\partial \eta}\frac{2}{h_2}\frac{2}{h_2}\frac{\partial \phi_j}{\partial \eta}J\,\mathrm{d}\xi\,\mathrm{d}\eta$$

$$\int \sum U_k\phi_k\frac{\partial \phi_i}{\partial \xi}\frac{\partial \phi_j}{\partial \eta}\,\mathrm{d}\xi\,\mathrm{d}\eta = \sum\left(U_k\int \psi_m\frac{\partial \psi_p}{\partial \xi}\psi_r\,\mathrm{d}\xi\int \psi_n\psi_q\frac{\partial \psi_s}{\partial \eta}\,\mathrm{d}\eta\right)$$

All these 1-D integrals are evaluated using the 1-D Gauss quadrature rule.

We have recast all the entries of coefficient matrix except C_{ij}^{00}, which we calculate using the 2-D Gauss quadrature.

5.1. Computer implementation

In multidimensions, shape functions are constructed by taking tensor product of 1-D shape functions. To use orthogonality we again separate them into 1-D shape functions. In 1-D we have vertex and interior modes. All the derivation presented earlier is for interior modes consisting of Jacobi polynomials. Shape functions for the vertex modes can be written as

$$\left(\frac{1-\xi}{2}\right) = \frac{1}{2}\left(P_0^{1,1} - \frac{P_1^{1,1}}{2}\right)$$

Thus, vertex modes in 1-D can be written as $\frac{1}{2}(P_0^{1,1} - \xi_i P_1^{1,1}/2)$, where ξ_i takes the values of ± 1. Now previous derivations can be used for vertex modes also.

6. IMPLEMENTATION OF BOUNDARY CONDITIONS

Since the modal basis functions do not satisfy interpolation and partition of unity properties, boundary conditions must be interpolated using some technique. Here, the boundary conditions

DOI: 10.1002/fld

are implemented using the least-squares method. Suppose $u = f(x)$ on Γ. We approximate $f(x)$ with $g(x)$ such that

$$f(x) \approx g(x) = \sum_{j=0}^{n} C_j \phi_j(x)$$

where ϕ_j are the same shape functions that are used to interpolate dependent variables in our formulation. Above equation is written for an element boundary Γ_e that coincides with domain boundary Γ. We assemble global coefficient matrix obtained by this equation as

$$E = g(x) - f(x)$$

$$E^2 = (C_j \phi_j - f, C_k \phi_k - f)$$

We minimize the square of the error with respect to C_j and obtain

$$\frac{\partial (E)^2}{\partial C_k} = 2(C_j \phi_j - f, \phi_k) = 0$$

$$\Rightarrow \ (C_j \phi_j, \phi_k) = (f, \phi_k) \ \Rightarrow \ \underline{A} C = B$$

where

$$A_{kj} = (\phi_k \phi_j) = \int \phi_j(x) \phi_k(x) \, \mathrm{d}x$$

$$B_k = (f, \phi_k) = \int f(x) \phi_k(x) \, \mathrm{d}x$$

7. TIME-DEPENDENT PROBLEMS

For time integration, space–time coupled or space–time decoupled methods can be used. Here, we consider space–time decoupled formulations. In space–time decoupled formulations, discretization in space and time are carried out independently. Generally, the time derivatives are represented by a truncated Taylor series in time. Least-squares functional for backward multi-step scheme of order M_α can be written as

$$\mathscr{J}(\mathbf{u}, p, \boldsymbol{\omega}; \mathbf{f}) = \frac{1}{2} \left(\left\| \frac{\gamma_0}{\Delta t} \mathbf{u}^{s+1} - \sum_{q=0}^{M_\alpha - 1} \frac{\beta_q}{\Delta t} \mathbf{u}^{s-q} + (\mathbf{u}_0 \cdot \nabla)\mathbf{u} + \nabla p + \frac{1}{Re} \nabla \times \boldsymbol{\omega} - \mathbf{f} \right\|^2_{0,\Omega \times (0,\tau]} \right.$$

$$\left. + \|\boldsymbol{\omega} - \nabla \times \mathbf{u}\|^2_{0,\Omega \times (0,\tau]} + \|\nabla \cdot \mathbf{u}\|^2_{0,\Omega \times (0,\tau]} \right) \tag{28}$$

where $\gamma_0 = \sum_{q=0}^{M_\alpha - 1} \beta_q$ for consistency, β_q are weights associated with a particular multi-step scheme, $\Delta t = t_{s+1} - t_s$ is the time increment.

DOI: 10.1002/fld

8. NUMERICAL EXAMPLES

In this section, we present numerical results obtained with the proposed formulation. First, we verify spectral convergence. Next, we present results for the transient 2-D flow over a backward-facing step and steady flow past a circular cylinder at low Reynolds number.

8.1. Verification: Kovasznay flow

The benchmark problem to be used for the purpose of verification of the least-squares-based finite element models is an analytical solution to the 2-D steady incompressible Navier–Stokes due to Kovasznay [17]. Domain of interest is $\bar{\Omega} = [-0.5, 1.5] \times [-0.5, 1.5]$. The solution is given by

$$u = 1 - e^{\lambda x} \cos(2\pi y) \tag{29}$$

$$v = \frac{\lambda}{2\pi} e^{\lambda x} \sin(2\pi y) \tag{30}$$

$$p = p_0 - \tfrac{1}{2} e^{2\lambda x} \tag{31}$$

where $\lambda = Re/2 - (Re^2/4 + 4\pi^2)^{1/2}$ and p_0 is a reference pressure (an arbitrary constant).

We perform a p-refinement study. We fix spatial discretization and systematically increase the order of polynomial used in each element. The discretization is a non-uniform mesh of eight quadrilateral finite elements. We choose the L_2 least-squares functional as error measure. Convergence of this measure to zero implies that the L_2 norm of the governing equations converges to zero.

We use eight non-uniform quadrilateral elements for spatial discretization. The exact solution given by Equations (29) and (30) is used to prescribe Dirichlet boundary conditions. The system is linearized using Picard's method (direct iteration method) and the resulting symmetric positive-definite (SPD) system of equations are solved using conjugate gradient method with Jacobi preconditioner. Nonlinear convergence is declared when $\sum_{n=1}^{ndf} \|\Delta \mathbf{U}_n\| / \|\mathbf{U}_n\|$ is less than 10^{-4}, where ndf is the total number of degrees of freedom in the mesh and $\mathbf{U}$ is the solution vector (includes all degrees of freedom at a node). Convergence of conjugate gradient is declared when error is less than 10^{-6}.

Figure 4(a) shows streamlines for Kovasznay flow and Figure 4(b) shows pressure contours. To verify spectral convergence, we plot L_2 norm of least-squares functional $\mathscr{J}$ against polynomial order for vorticity-based first-order formulation in Figure 5. On logarithmic-linear scale we get almost straightline showing exponential decay of least-squares functional.

8.2. Transient flow over a backward-facing step

We next consider a 2-D flow over a backward-facing step at $Re = 800$. The geometry and boundary conditions are taken from the benchmark solution of Gartling [12] and they are shown in Figure 6. No-slip boundary condition is imposed on all walls. Boundary condition of $u(y) = 0$ is imposed for $-0.5 \leqslant y \leqslant 0.0$. A parabolic velocity profile given by $u(y) = 24y(0.5 - y)$ is specified at the inlet for $0.0 \leqslant y \leqslant 0.5$. This produces a maximum inflow velocity of $u_{\max} = 1.5$ and a mean inflow velocity of $u_{\text{avg}} = 1.0$. The Reynolds number is based on the mean inflow velocity. We impose outflow boundary condition in a weak sense through the least-squares functional [3]. For long domains, the strong outflow boundary condition $p = 0$ also gives good results. However, we prefer

DOI: 10.1002/fld

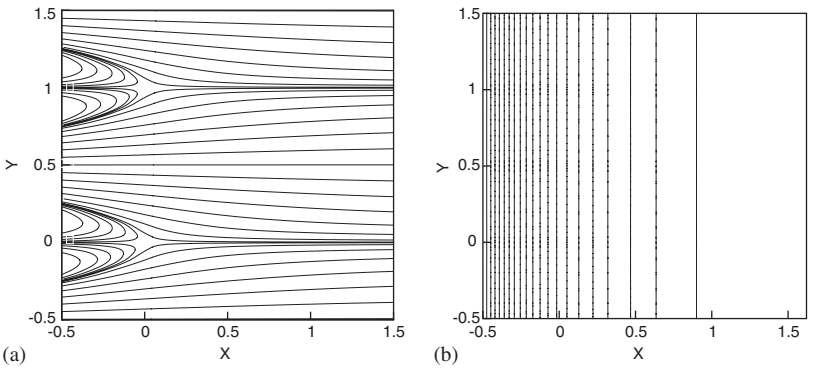

Figure 4. Kovasznay flow: (a) streamlines; and (b) pressure contours for $Re = 40$.

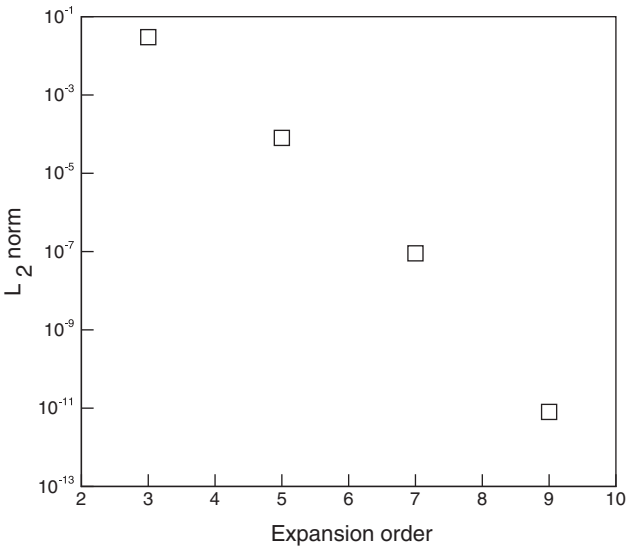

Figure 5. Delay of least-squares functional with polynomial order.

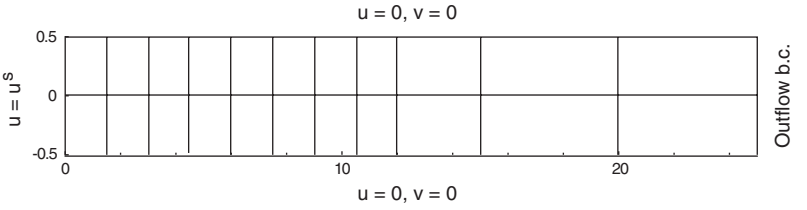

Figure 6. Mesh and boundary conditions for flow over a backward-facing step.

DOI: 10.1002/fld

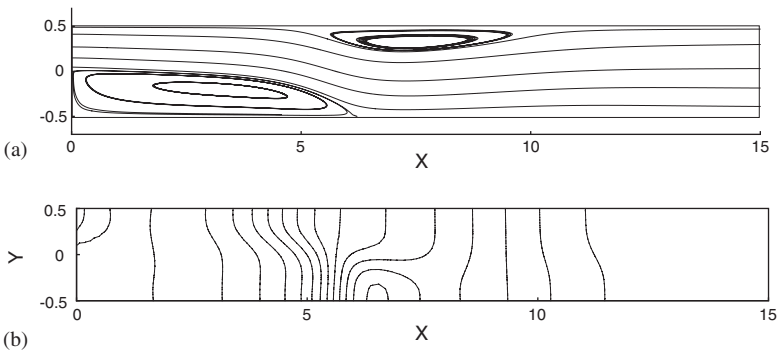

Figure 7. Flow over a backward-facing step at $Re = 800$: (a) streamlines; and (b) pressure contours.

the weak imposition of outflow boundary conditions. Initial condition is zero velocity everywhere in the domain.

The domain, $\bar{\Omega} = [0, 25] \times [-0.5, 0.5]$, is discretized using 22 finite elements as shown in Figure 6. To accurately resolve the primary and secondary circulation zones, we use a non-uniform grid. A ninth-order modal expansion is used in each element, resulting in a total of 7600 degrees of freedom in the mesh. The resulting discrete model is linearized using Picard's method. At each Picard step, the linear system of equations, involving a SPD coefficient matrix, is solved using the conjugate gradient method with a Jacobi preconditioner. Convergence of the conjugate gradient method is declared when the norm of the residual is less than 10^{-6}. Nonlinear convergence is declared when the relative norm of the residual in solution vector is less than 10^{-4}. A time increment of 0.2 is used to march in time.

Figure 7 shows the streamlines and pressure contours for $0 \leqslant x \leqslant 15$, where most of the phenomena of interest occur. The primary reattachment length is approximately 6.10, while the secondary separation and reattachment lengths approximately 4.9 and 10.4, respectively. Figure 7(b) shows the pressure contours. After reattachment of the upper wall eddy, the flow slowly recovers towards a fully developed Poiseuille flow. The flow is almost fully developed at the exit with no pressure gradient in y direction. This is because the outlet boundary condition of $p = 0$ also gives identical results.

Figure 8 shows evolution of velocity field with time. The main flow coming from the inlet follows a sinuous path, forming a series of eddies along the upper and lower wall. Initial velocity field is taken to be zero everywhere in the domain. At $t = 400$, the relative norm of the residual in velocities between two consecutive time steps was less than 10^{-4}, indicating that a steady state was achieved.

Figure 9 shows a plot of the L_2 least-squares functional as a function of time. Initially, there is some fluctuation but fluctuations damp with time and the functional stabilizes at a value of 3×10^{-3}.

8.3. Steady flow past a circular cylinder at low Reynolds number

Next, we consider steady 2-D flow of an incompressible fluid past a circular cylinder. The Reynolds number is taken to be 40, for which a steady-state solution exists. Domain of interest is $[-10.0, 15.0] \times [-10.0, 10.0]$. The x-component of inlet velocity (u) is specified to be 1.0 and

DOI: 10.1002/fld

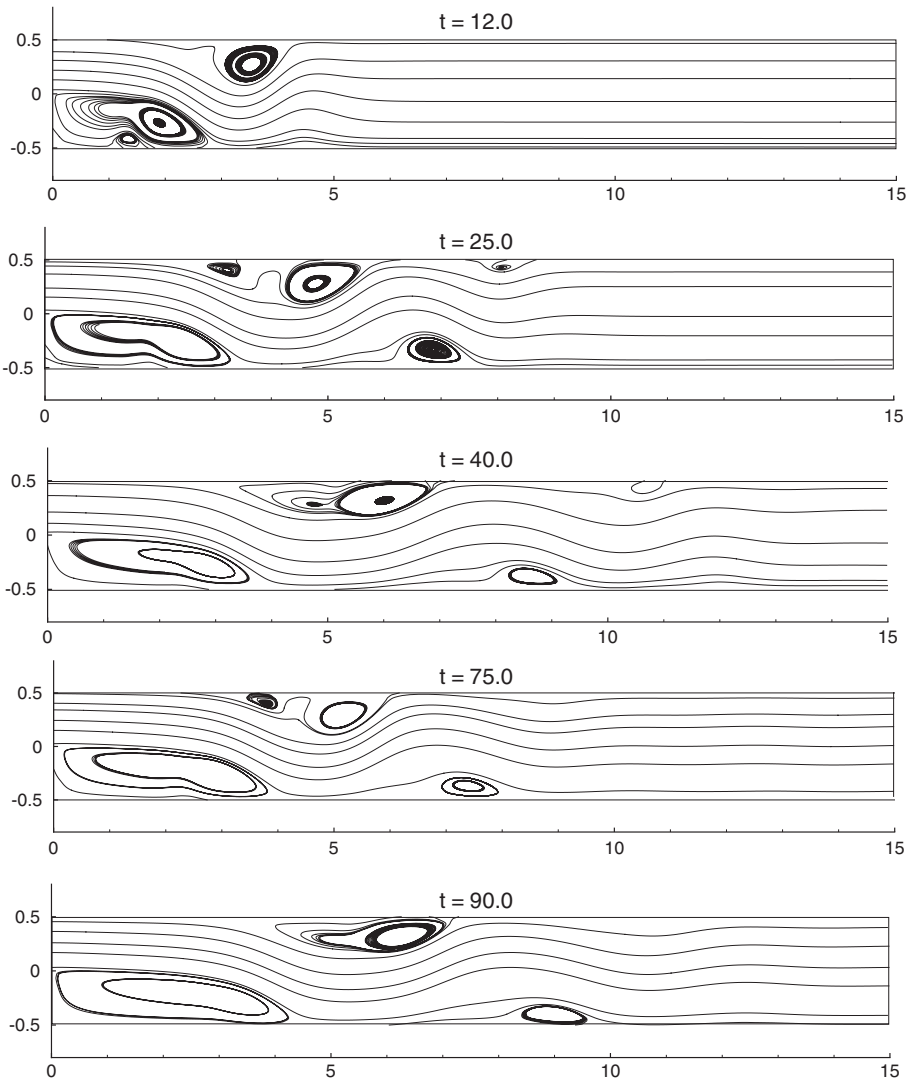

Figure 8. Time history streamline plots for flow over a backward-facing step at $Re = 800$.

the y-component (v) is set to zero. Symmetry boundary conditions, $\omega_z = 0$ and $v = 0$, are imposed on the top and bottom walls. The outflow boundary conditions are imposed in a weak sense through the least-squares functional.

Figure 10 contains a close-up view of the geometric discretization around the circular cylinder. We generate orthogonal grid (rectangular elements) everywhere in the domain except around the cylinder. One layer of body fitting grid is generated around the cylinder. In order to accurately represent the curved boundary, we implement an isoparametric formulation; i.e. we use the same expansion order to interpolate dependent variables and the geometry.

DOI: 10.1002/fld

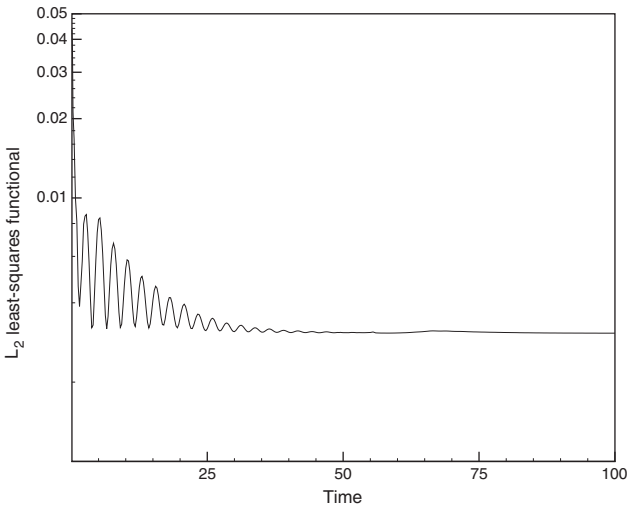

Figure 9. Time history of the L_2 least-squares functional.

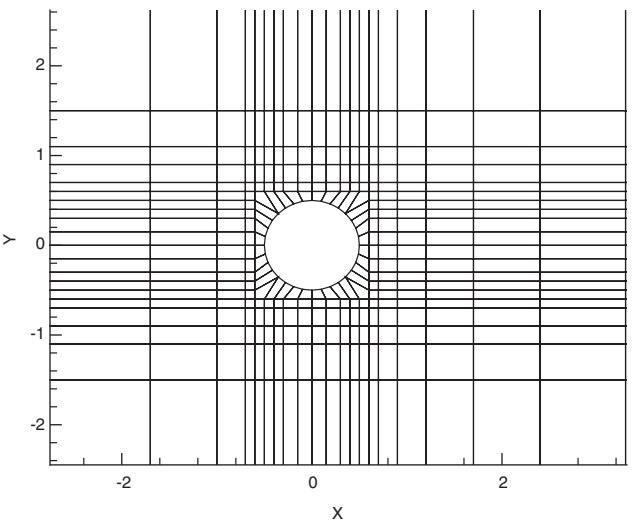

Figure 10. Close-up view of geometric discretization around the cylinder.

We use 2-D steady incompressible Navier–Stokes equations in the vorticity-based first-order form and with a ninth-order modal expansions in each element. The resulting discrete model consists of a total of 209 196 degrees of freedom. The value of the L_2 least-squares functional remains below 10^{-4}.

Figures 11 and 12 contain plots of the contours of streamlines and pressure, respectively, in the wake region for $Re = 40$. The value of the recirculation length is found to be 4.55 cylinder radius. The present result is in good agreement with the numerical value of 4.55 cylinder

DOI: 10.1002/fld

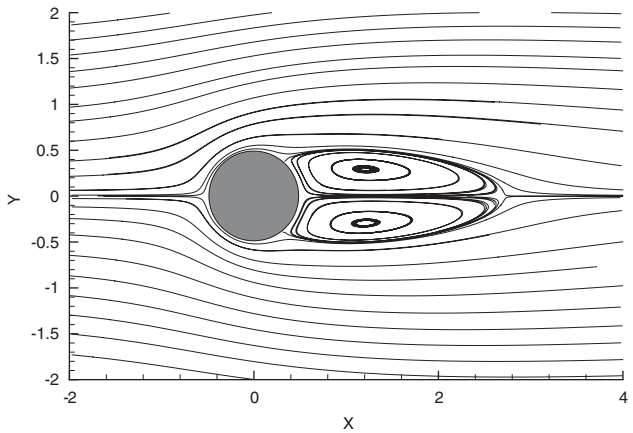

Figure 11. Streamlines in the wake region for flow past a circular cylinder at $Re = 40$.

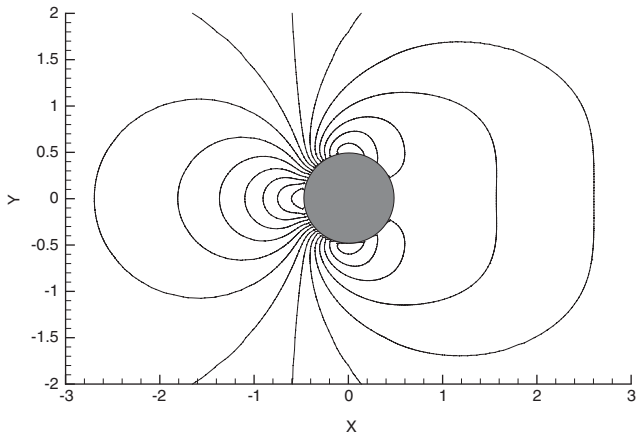

Figure 12. Pressure contours for flow past a circular cylinder at $Re = 40$.

radius by Pontaza and Reddy [3]. Dennis and Chang [18] reported a recirculation length of 4.69 cylinder radius.

A comparison of the experimental values of the surface pressure coefficient distribution along the cylinder surface with the computed values is shown in Figure 13. Experimental values are taken from Grove *et al.* [13]. The present results are in good agreement with the experimental measurements. Drag coefficient is calculated to be $C_D = 1.55$, which is in good agreement with the published results of Tritton [19], who reported a value of 1.56.

Actual CPU time depends on the implementation (data structure, node numbering, etc.) and vary from one implementation to other. To give the reader a feeling of the algorithmic performance, we report the speed-up obtained by using proposed orthogonal modal bases.

DOI: 10.1002/fld

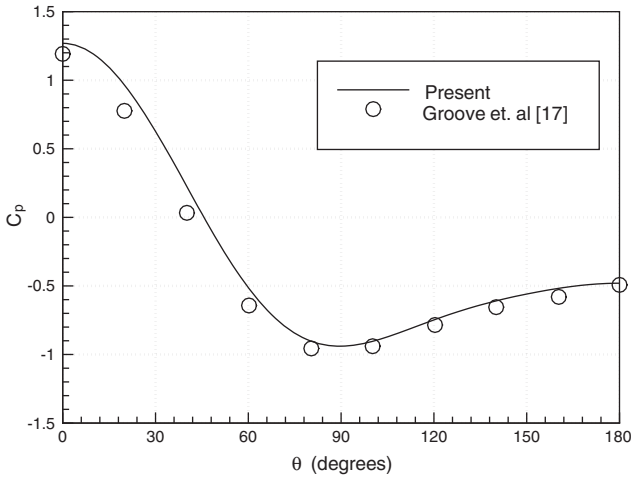

Figure 13. Pressure coefficient distribution along the cylinder surface for flow past a circular cylinder at $Re = 40$.

Polynomial order (P)	Speed-up ($t_{\text{non-ortho}}/t_{\text{ortho}}$)
7	2.1
9	3.1
11	4.5

At this point, we want to remind the reader that we recast all the terms of coefficient matrix except C_{ij}^{00} term associated with rectangular elements. We evaluated C_{ij}^{00} using the 2-D Guass quadrature. Calculation of other nonlinear terms C_{ij}^{01}, C_{ij}^{02}, C_{ij}^{10}, C_{ij}^{20} is also computationally expensive as they involve do-looping even though we calculate them by performing 1-D Gauss quadrature. Most of the time is consumed in computing these terms only. For curved elements, we performed 2-D Guass quadrature for all the terms of coefficient matrix.

9. CONCLUDING REMARKS

In this paper, a method to exploit orthogonality of modal bases in order to avoid numerical integration and have a fast computation is presented. The entries of coefficient matrix are calculated analytically. The properties of Jacobi polynomials are used and most of the entries of coefficient matrix are recast so that they can be evaluated analytically. This strategy is implemented in the context of least-squares finite element model, although this procedure can be used in other finite element formulations. The equations are linearized using direct iteration method (Picard method). Analytical expressions are developed for rectangular elements. Spectral convergence of the L_2 least-squares functional is verified using the exact solution of the Kovasznay flow. Numerical results are presented for unsteady flow over a backward-facing step. Also, the steady flow past a circular cylinder is analysed and it showed reduction in computational cost.

DOI: 10.1002/fld

All the terms of coefficient matrix were recast except C_{ij}^{00} term. This term was evaluated using the 2-D Guass quadrature. Also the 1-D Gauss integration is performed for $((\partial\psi/\partial\xi)\partial\psi/\partial\xi)$, which is quite fast as it is 1-D integration, and 2-D and 3-D expressions $((\partial\psi/\partial\xi)\partial\psi/\partial\xi)$ can be calculated by making use of the 1-D expression without the use of numerical integration. Other than these two Gauss quadratures, no numerical integration is used to evaluate the coefficients.

Limitation of this procedure is that it can be used only for rectangular elements. For skew elements, it is not possible to separate multidimensional integrals (entries) into 1-D integrals. Therefore, one may choose to use analytical expressions to evaluate entries for rectangular elements and use quadrature for curved elements.

ACKNOWLEDGEMENTS

The authors gratefully acknowledge the support of this work by the Computational Mathematics Program of the Air Force Office of Scientific Research through Grant F49620-03-1-0201.

REFERENCES

1. Pontaza JP, Reddy JN. Space–time coupled spectral/*hp* least-squares finite element formulation for the incompressible Navier–Stokes equations. *Journal of Computational Physics* 2004; **197**:418–459.
2. Karniadakis GE, Sherwin SJ. *Spectral/hp Element Methods for CFD*. Oxford University Press: Oxford, 1999.
3. Pontaza JP, Reddy JN. Spectral/*hp* least-squares finite element formulation for the Navier–Stokes equations. *Journal of Computational Physics* 2003; **190**:523–549.
4. Prabhakar V, Reddy JN. Spectral/*hp* penalty least-squares finite element formulation for the steady incompressible Navier–Stokes equations. *Journal of Computational Physics* 2006; **215**:274–297.
5. Peano A. Hierarchies of conforming finite elements for plane elasticity and plate bending. *Computers and Mathematics with Applications* 1976; **2**:211–224.
6. Szabo BA, Babuska I. *Finite Element Analysis*. Wiley: New York, 1991.
7. Dubiner M. Spectral methods on triangles and other domains. *Journal of Scientific Computing* 1991; **6**:345–390.
8. Sherwin SJ, Karniadakis GE. A triangular spectral method: applications to the incompressible Navier–Stokes equation. *Computer Methods in Applied Mechanics and Engineering* 1995; **123**:189–229.
9. Patera AT. A spectral method for fluid dynamics: laminar flow in a channel expansion. *Journal of Computational Physics* 1984; **54**:468–488.
10. Warburton TC, Sherwin SJ, Karniadakis GE. Basis functions for triangular and quadrilateral high-order elements. *SIAM Journal on Scientific Computing* 1999; **20**:1671–1695.
11. Zienkiewicz OC, Taylor RL. *The Finite Element Method*, vol. 1. McGraw-Hill: New York, 1989.
12. Gartling DK. A test problem for outflow boundary conditions—flow over a backward-facing step. *International Journal for Numerical Methods in Fluids* 1990; **11**:953–967.
13. Grove AS, Shair FH, Petersen EE, Acrivos A. An experimental investigation of the steady separated flow past a circular cylinder. *Journal of Fluid Mechanics* 1964; **19**:60–80.
14. Osilenker B. *Fourier Series in Orthogonal Polynomials*. World Scientific: Singapore, 1999.
15. Reddy JN. *An Introduction to the Finite Element Method* (3rd edn). McGraw-Hill: New York, 2006.
16. Reddy JN. *Introduction to Nonlinear Finite Element Analysis*. Oxford University Press: Oxford, 2004.
17. Kovasznay LSG. Laminar flow behind a two-dimensional grid. *Mathematical Proceedings of the Cambridge Philosophical Society* 1948; **44**:58–62.
18. Dennis SCR, Chang GZ. Numerical solutions for steady flow past a circular cylinder at Reynolds numbers up to 100. *Journal of Fluid Mechanics* 1970; **42**:471–489.
19. Tritton DJ. Experiments on the flow past a circular cylinder at low Reynolds numbers. *Journal of Fluid Mechanics* 1959; **6**:547–567.

DOI: 10.1002/fld